Hybrid Ab-Initio/Empirical Molecular Dynamics: Combining the ONIOM Scheme with the Atom-Centered Density Matrix Propagation (ADMP) Approach

Nadia Rega, Srinivasan S. Iyengar,† and Gregory A. Voth*

Department of Chemistry and Henry Eyring Center for Theoretical Chemistry, 315 S. 1400 E, Room 2020, University of Utah, Salt Lake City, Utah 84112-0850

H. Bernhard Schlegel

Department of Chemistry, Wayne State University, Detroit, Michigan 48202-3489

Thom Vreven and Michael J. Frisch

Gaussian, Inc., 140 Washington Avenue, North Haven, Connecticut 06473-1712

Received: October 11, 2003; In Final Form: January 26, 2004

A new methodology to perform hybrid empirical/ab-initio molecular dynamics is presented. The method combines the well-established hybrid ONIOM scheme with the recently developed ADMP (Atom-Centered Density Matrix Propagation) approach, where the one electron density matrix expanded in an atom-centered Gaussian basis set is propagated as electronic variables along with the classical nuclear degrees of freedom via an extended Lagrangian procedure. The unified and single-valued ONIOM expressions for the energy and energy derivatives allow for an implementation of conservative dynamics. It is found that atom-centered basis sets large enough to provide good chemical accuracy can be used even when electronic embedding is adopted in the QM/MM scheme, and this does not affect the well-behaved and conservative nature of the dynamics. The method contains very appealing features for the study of biological systems, including the ability to employ accurate density functionals, the freedom to choose a periodic or a cluster boundary condition for the system under study, asymptotic O(N) scaling through established techniques, and the ability to use reasonably large time-steps through the tensorial fictitious mass scheme. The general ADMP/ONIOM formalism is illustrated through a series of test calculations. A simulated study of proton hopping inside the gramicidin A ion channel is also presented, to show the potential of the method in describing reactivity in large systems.

I. Introduction

The combination of different levels of theory in hybrid methods constitutes a powerful tool often exploited to study complex molecular systems. In particular, the motivation of combining quantum-mechanical and empirical models is well-known:[1−3] the representation of a large system like a protein is typically carried out at the molecular mechanics level for reasons of efficiency, but the modeling of processes such as bond-making or bond-breaking often requires quantum mechanical methods. Fortunately, the region of space affected by important changes in electronic structure is usually relatively small when compared to the size of the whole system under study. Thus, the explicit representation of electrons may be necessary for only a limited portion of the system, while important environmental effects, that would be absent in reduced models, can be taken into account using empirical methods. Steric effects and long-range interactions in enzymes and in liquids are typical examples of complex structure and dynamics for which mixed methods offer a good compromise between accuracy and feasibility for theoretical investigations.

Potential energies obtained from mixed quantum-mechanics (QM) and molecular mechanics (MM)[4−10] have been used in several versions of Born−Oppenheimer (BO) dynamics,[4−6] where the quantum mechanical calculations require the solution of the Hamiltonian eigenvalue problem at each time step of the propagation. Because of this bottleneck, the calculation of the energy and forces on the fly is usually limited to semiempirical methods for large systems such as the active site of an enzyme, which may involve tens to thousands of atoms. Semiempirical methods are also the most common, but often an unsatisfactory, choice to obtain reactive paths connecting stationary points of the hybrid energy surface.[7,8]

Extended Lagrangian[11,12] ab-initio dynamics[13−20] are particularly well suited to simulate systems characterized by a large number of degrees of freedom and governed by hybrid potentials. In this approach the electronic information does not rely on the solution of a self-consistent field procedure, but is propagated along with the classical nuclear degrees of freedom by an adjustment of the relative time scales of the electronic and nuclear motion. The combination of a hierarchical picture for the molecular energy together with the use of dynamic variables to mimic the electronic evolution promises to enable us to investigate the potential energy surface for large biomolecular systems at a high level of accuracy and in a computationally efficient manner. The QM/MM versions of the Car-Parrinello (CP) method belong to this category.[21−24] The QM part, composed of Kohn−Sham orbitals expanded in a plane wave basis set and propagated together with the nuclei, is

* Corresponding Author. E-mail: voth@chemistry.utah.edu.
† Present address: Department of Chemistry, Indiana University, 800 E. Kirkwood Ave., Bloomington, IN 47405.

10.1021/jp0370829 CCC: $27.50
Published on Web 03/10/2004

combined with MM calculations consisting of classical dynamics using empirical force fields. However, the use of delocalized plane-wave basis functions in a QM/MM system renders the choice of box size to be extremely critical, since the QM system can be thought of as a cluster placed in an MM environment. As noted in ref 15, neutral clusters are generally treated in plane wave basis sets using the super-cell method, where the size of the cell is made large so that the periodic images do not interact with each other. This, however, can lead to serious issues within a QM/MM scheme where a large box might result in MM atoms (and charges) being present inside the supercell box where the basis functions have nonzero amplitudes. On the contrary, making the plane-wave box size small also has serious repercussions on account of artifacts from periodic boundary conditions. Charged molecular clusters in a vacuum (in the absence of MM atoms that might be present in a QM/MM treatment) have been treated[15] using plane-waves, by explicitly removing the long-range electrostatic contributions of the charged species by integrating the Poisson equation. By contrast, the implementation of the correct physical boundary conditions for a localized QM system is more natural with atom-centered basis functions and very little special care is necessary.

In this paper we wish to present a novel methodology to perform a combined ab-initio/empirical molecular dynamics based on an extended Lagrangian approach. To this end, the recently developed ADMP (Atom-centered basis functions Density Matrix Propagation) ab-initio dynamics method[16−20] is combined with the ONIOM[25−33] approach to perform hybrid potential calculations.

ONIOM is a method for combining calculations using a high level of theory on a part of a large system with lower level calculations on the full system. In its full generality, ONIOM can combine several levels of theory and corresponding model systems within one calculation. However, the present work focuses on using two levels of theory, one a quantum mechanical (MO) method and the other Molecular Mechanics—ONIOM(MO:MM)—to produce a particular QM/MM method. The ONIOM QM/MM model is distinguished from most QM/MM models in two ways:

1. ONIOM uses additivity to integrate the energies (and other properties, such as energy derivatives) from the constituent models, rather than solving a problem involving one Hamiltonian containing terms from the different models. Consequently, the individual calculations which contribute involve standard QM or MM methods, allowing all the existing functionality for calculations on the uncorrected model system to be carried over. In particular, any QM method can be used with ONIOM(MO:MM) and the implementation of ADMP for the pure MO case carries over virtually unchanged to the ONIOM(MO:MM) case.

2. The coordinates of the link atoms required when bonds are truncated to form the model system are well-defined functions of the Cartesian coordinates of the atoms in the bond in the real system, so that all component energies are smooth functions of the coordinates of the atoms in the real system. Consequently, potential energy surfaces for the ONIOM integrated energy are well-defined, and it is possible to conduct dynamics using the ONIOM energies and forces.

QM/MM models have a long history[1−3] and have been used for dynamics on the Born−Oppenheimer surface since their inception. More recently, Ziegler and co-workers have used their variant of the earlier IMOMM method of Morokuma to perform CP dynamics.[23,24]

A good ONIOM model should produce (a) results for properties which primarily involve atoms in the model system which are similar to those predicted by the high-level calculation applied to the real system, and which are closer to the high-level calculation on the real system than the uncorrected high-level calculation on the model system, and (b) results for properties involving the other atoms which are no worse than the low-level calculation on the real system. Morokuma and co-workers have also introduced a novel QM/MM scheme to facilitate more efficient Born−Oppenheimer dynamics.[34] This approach allows for exchange of particles between the two layers, by introduction of a buffer zone, and results in a dynamics scheme that is shown to conserve energy.

In the ADMP approach, the one-electron density matrix is expanded in an atom-centered (Gaussian) basis and is propagated as electronic variables. A comparative study of ADMP and Born−Oppenheimer dynamics[18] has shown that the current implementation of ADMP is a factor of 4 faster than Born−Oppenheimer dynamics[18] for each time-step. Born−Oppenheimer dynamics can, at the most, allow a time-step twice as large as that allowed in ADMP[18] while maintaining similar energy conservation when the same integrator (velocity Verlet) is used. This is on account of reasonably large time-steps already allowed within ADMP through efficient use of the tensorial fictitious mass scheme.[17] This renders the current implementation of ADMP within the Gaussian suite of electronic structure codes[35] to be at least a factor of 2 faster than Born−Oppenheimer dynamics for a given total trajectory time. This offers computational advantages over other semiempirical/MM Born−Oppenheimer dynamics methods for QM/MM dynamics. In comparison to traditional semiempirical/MM Born−Oppenheimer dynamics, ADMP is more efficient when using the same QM model and ADMP can be applied using more accurate QM models, including Hartree−Fock and pure or hybrid DFT. The latter is particularly important for studies of reactivity in biological systems, because semiempirical methods have limited accuracy for transition state structures and reaction paths, especially when transition metals are involved. In comparison to the CP method using a plane wave basis, ADMP has the advantage of being able to employ hybrid density functionals, which are known to be of substantially better accuracy in describing activation energies, especially when motion of hydrogens is involved, and in describing hydrogen bonds.

Another important advantage is that atom-centered functions can be used with the correct physical boundary conditions for molecules, polymers, surfaces, and solids, without the need to treat replicated cells in order to impose 3d periodicity. Consequently, charged systems and QM/MM models can be treated as easily as neutral molecules and long-range interactions can be introduced using periodic boundary conditions. Alternatively, the QM/MM system can be treated as a cluster where different layers interact to a small, even if significant, extent, and long-range interactions can be included using a suitable continuum solvent model.

Another crucial issue when hybrid methods are employed to treat large systems is the computational efficiency. The ADMP/ONIOM approach shows an asymptotic O(N) scaling by virtue of established techniques[36] and the capability of employing reasonably large time-steps through the use of a tensorial fictitious mass. Finally, ADMP allows one to treat all electrons in the QM region of the system explicitly without resorting to pseudopotentials (unless so desired), and to systematically control the deviation from the Born−Oppenheimer surface and the resulting mixing of fictitious and real kinetic energies. It must be noted here that the Projector-Augmented Wave (PAW)[37] approach and novel Car-Parrinello schemes using both Gaussian

and Plane wave basis sets[38,39] can also allow the treatment of core electrons, although not in as complete a fashion as is possible within the ADMP approach. In this regard, it is particularly interesting to discuss a new approach to the CP scheme[40] that uses Wannier basis functions[41,42] instead of plane waves to represent the electronic structure. The Wannier basis functions[41,42] are unitary transforms of the plane-wave basis sets, generated under the condition of maximal spatial localization of the resultant basis functions. In ref 40, the Wannier basis functions are used to represent the CP orbitals, and these basis functions are propagated simultaneously along with the molecular orbital coefficients using the same fictitious mass as the molecular orbital coefficients. In this regard, this approach is quite similar to the floating Gaussian approach to Car-Parrinello dynamics[43] where Gaussian basis function centers and widths are simultaneously propagated using a fictitious mass.

The present paper is organized as follows. In Section 2, the ADMP/ONIOM algorithm is described. Section 3 is then dedicated to the discussion of a few applications aimed at validating the accuracy and stability of the simulations and the reliability of the QM/MM interface coupling of the ONIOM potential. We also present preliminary results of a study currently in progress on the proton translocation inside the ion channel gramicidin A, to show the potential of the method in describing reactivity in large systems. Concluding remarks are then provided in Section 4.

II. The ADMP/ONIOM Molecular Dynamics Algorithm

A. The ONIOM Potential Energy Surface. In the ONIOM scheme, the energy of a system as a whole is expressed as a linear combination of subsystems of different size and at different levels of theory. Here we consider the simplest form of such an approach, involving the definition of a *core* portion (the *model* system) of the entire system (the *real* system), and the ONIOM combination of QM and MM levels of description yields the expression

$$E^{\mathrm{ONIOM}} = E^{\mathrm{MM,real}} - E^{\mathrm{MM,model}} + E^{\mathrm{QM,model}} \qquad (1)$$

Note that the real system is treated only at the MM level, while the model is considered at both the MM and QM levels. The model is chosen to capture all of the important quantum effects which determine, for example, chemical bond-breaking and formation or rapid change of the electronic polarization.

Once the atoms whose interactions require the quantum mechanical description have been chosen, the complete model system is generated in one of two ways:

1. The model system includes (a) the selected atoms and (b) additional link atoms, typically hydrogens, which terminate bonds between selected atoms and unselected atoms. This is usually termed mechanical embedding, since the coupling between the model system and the real one is solely due to the molecular mechanics terms in the MM calculation on the real system.

2. The model system includes the selected atoms and the link atoms as in mechanical embedding, and all real system atoms not selected and not replaced by link atoms are replaced by point charges at the same location. This is usually termed electronic embedding, because the electronic structure in the QM calculation is affected by the charges of the full system. The point charges are typically the same charges used in the MM calculation on the real system, except that to avoid over-polarization effects, the charges for atoms within a few bonds of the link atoms are scaled down or set to zero. Note that both the QM and MM calculations use the same model system, including the point charges. Consequently, the Fock matrix in the QM calculation depends on the coordinates of all atoms in the real system, and there are nonzero contributions to the forces on all atoms in the real system from each model system calculation.

All results reported here use electronic embedding, and the point charges in the model system for atoms which are either bonded to a link atom or are one bond further removed from a link atom are set to zero.

It should be noted that the electronic embedding may be regarded as being possibly incomplete when nonpolarizable MM force fields are employed. However, average polarization effects can be included to a certain amount even in force fields not containing explicit polarization terms, if the parameters are properly fitted to the experiment.[44] In addition, recently developed models such as the Effective Fragment Potential (EFP) approach[45] can be used in the current scheme, and such models could improve the quality of the MM region on account of a detailed inclusion of polarization effects. However, no polarizable force field seems to be yet available which has a complete parametrization and has been systematically tested on biological systems.

An essential ingredient in the definition of hybrid energy potentials is the methodology adopted if chemical bonds intersect the boundary between different layers. When artificial atoms saturate the dangling valences of the model across the boundary (link atoms approach[46]), the correct number of degrees of freedom and therefore the unique definition of the potential energy are ensured by defining the coordinates of the link atom as follows:[31−33]

$$\mathbf{r}_{\mathrm{link}} = \mathbf{r}_{\mathrm{bond}} + g(\mathbf{r}_{\mathrm{sub}} - \mathbf{r}_{\mathrm{bond}}) \qquad (2)$$

where $\mathbf{r}_{\mathrm{bond}}$ is the position of the model atom to which the link is bonded to substitute the atom belonging to the surrounding region and located in $\mathbf{r}_{\mathrm{sub}}$. In eq 2, g is a scale factor, normally set to $R(\mathrm{M-L})/R(\mathrm{M-R})$, where $R(\mathrm{M-L})$ is a typical bond length between the model system atom and the link atom (H in all cases in this work), and $R(\mathrm{M-R})$ is a typical bond length for the pair of atoms in the real system. Careful tests have shown that the ONIOM results are quite insensitive to the value of g.[30] It must be stressed that, since the link atom positions are fully defined by the coordinates of the real system, the ONIOM energies and gradients can be written as functions of only real nuclei positions **R**. Thus, the ONIOM potential as defined in (1) and (2) is single valued and differentiable with respect to **R**, allowing conservative dynamics to be performed.

In the following subsection we shall describe the implementation of ADMP dynamics on an ONIOM potential energy surface involving link atoms (eqs 1 and 2) and with electronic embedding to treat electrostatic QM/MM interactions in non-polarizable force fields.

B. The ADMP Dynamics Exploiting the ONIOM Potential. The ADMP/ONIOM extended Lagrangian governing the dynamics is formally identical to the Lagrangian exploited for full ab-initio propagation:

$$\mathcal{L}_{\mathrm{ADMP}} = \frac{1}{2}Tr(\mathbf{V}^{\mathbf{T}}\mathbf{M}\mathbf{V}) + \frac{1}{2}Tr([\mu^{1/4}\mathbf{W}\mu^{1/4}]^2) - E^{\mathrm{ONIOM}}(\mathbf{R},\mathbf{P}) - Tr[\Lambda(\mathbf{P}\mathbf{P} - \mathbf{P})] \qquad (3)$$

where the nuclei of the real system are propagated with coordinates **R**, velocities **V,** and masses **M**, while the electronic degrees of freedom of the model are propagated with the density

matrix **P**, the density matrix velocity **W**, and the density matrix fictitious mass tensor μ. In eq 3, **P** is the density matrix in an orthonormal Gaussian basis set, related to the corresponding matrix in the nonorthogonal basis, **P′**, by $\mathbf{P} = \mathbf{U}\mathbf{P}'\mathbf{U}^{\mathbf{T}}$, where **U** is the factorization matrix of the nonorthogonal basis overlap matrix $\mathbf{S}' = \mathbf{U}^{\mathbf{T}}\mathbf{U}$. The matrix **U** can be obtained by Cholesky decomposition[47] or Lowdin symmetric orthonormalization. The Lagrangian multiplier matrix Λ imposes constraints on the total number of electrons and the idempotency of the one-particle density matrix (the so-called N-representability constraints). Note that while **P** includes the electronic variables for the model only, the potential energy surface also depends on the molecular mechanics energy function through the set of parameters.

The formal identity with the full ab-initio dynamics holds also for the analysis of the deviations from the Born−Oppenheimer surface. The adiabatic performance of ADMP dynamics has been studied in some detail (see refs. 17, 19). In particular, the deviations depend on the magnitude of the commutator of the Fock and density matrixes [**F**,**P**] and on the fictitious mass μ. These quantities are found to be closely interrelated and the choice of the fictitious mass provides a lower bound on the deviations from the true BO surface.

The Euler−Lagrange equations of motion for the nuclei and density matrix expanded in the orthonormal basis set are

$$\mathbf{M}\frac{\mathrm{d}^2\mathbf{R}}{\mathrm{d}t^2} = -\left.\frac{\partial E^{\mathrm{ONIOM}}(\mathbf{R},\mathbf{P})}{\partial \mathbf{R}}\right|_{\mathbf{P}} \tag{4}$$

and

$$\mu^{1/2}\frac{\mathrm{d}^2\mathbf{P}}{\mathrm{d}t^2}\mu^{1/2} = -\left[\left.\frac{\partial E^{\mathrm{ONIOM}}(\mathbf{R},\mathbf{P})}{\partial \mathbf{P}}\right|_{\mathbf{R}} + \Lambda\mathbf{P} + \mathbf{P}\Lambda - \Lambda\right] \tag{5}$$

These equations can be integrated using the velocity Verlet algorithm,[48] while the Lagrangian multiplier matrixes are determined by an iterative scheme[16,17] so that $\mathbf{P}_{i+1}$ and $\mathbf{W}_{i+1}$ satisfy the idempotency constraint, $\mathbf{P}^2 = \mathbf{P}$, and its time derivative, $\mathbf{PW} + \mathbf{WP} = \mathbf{W}$.

The force acting on the density matrix (rhs of eq 5) has the same analytical form as in full ab-initio ADMP

$$\left.\frac{\partial E(\mathbf{R},\mathbf{P})}{\partial \mathbf{P}}\right|_{\mathbf{R}} = 3\mathbf{FP} + 3\mathbf{PF} - 2\mathbf{FP^2} - 2\mathbf{PFP} - 2\mathbf{P}^2\mathbf{F} \tag{6}$$

In the case of electronic embedding, the Fock matrix, **F**, includes electrostatic interactions with all the real system atoms.

The nuclear forces in eq 4 are obtained by a simple derivative of the energy expression in eq 1:

$$\left.\frac{\partial E^{\mathrm{ONIOM}}(\mathbf{R},\mathbf{P})}{\partial \mathbf{R}}\right|_{\mathbf{P}} = \frac{\mathrm{d}E^{\mathrm{MM,real}}(\mathbf{R})}{\mathrm{d}\mathbf{R}} - \frac{\mathrm{d}E^{\mathrm{MM,model}}(\mathbf{R})}{\mathrm{d}\mathbf{R}} + \left.\frac{\partial E^{\mathrm{QM,model}}(\mathbf{R},\mathbf{P})}{\partial \mathbf{R}}\right|_{\mathbf{P}} \tag{7}$$

The forces in the QM calculation are computed as described in refs 16, 17, 19, and the model system forces are transformed to real system forces as described in ref 29. It is, however, important to note here that the nuclear forces in ADMP involve additional terms that depend on the commutator of the Fock and density matrixes[16,19] unlike those in the standard ONIOM implementation[29] for Born−Oppenheimer dynamics.

The possible unphysical interaction between the QM electronic density and the MM nuclei in proximity to the QM/MM boundary is an important source of instability in dynamics governed by potentials mixing quantum models with empirical force fields. The MM charges polarize the QM electron density and this polarization depends on the proximity of the MM charges. In some situations, it may happen that the electronic basis functions that are used to describe the QM part may physically overlap with the MM positive charges. This could happen, for example, when largely delocalized atom-centered basis functions are used on the neighboring QM atoms, or when totally delocalized basis functions (such as plane waves) are used to describe the electronic structure. In either case, the presence of an MM charge inside the domain of a given basis function can create an artificial effect of drawing electrons close to that MM atom. This is especially true for a bare positive charge large enough so that an electron binds to it with more binding energy than the lowest ionization potential of the QM system. (A large negative charge may be expected to show the opposite effect.) As stated earlier, one aspect of this overpolarization can be taken into account by scaling down the MM charges in close proximity to the link atoms (i.e., those directly bonded to the substituted atom).[49,50] In the extended Lagrangian approach, a monitor of the overpolarization event is the heating of electronic variables. The one-electron matrix that enters into the forces acting on the density matrix in eq 6 as part of the Fock matrix includes interactions between the MM charges and the QM density, thus directly affecting the integration in the time of both the density matrix **P** and its velocity **W**. If MM charges come too close to the electronic density, the elements of the one-electron matrix increase in magnitude, leading to an artificial acceleration of electronic variables. As a consequence, unphysical dynamics can occur. (This would also affect the fictitious kinetic energy in ADMP dynamics.) Another estimate of this effect may be obtained by monitoring the value of the most diffuse basis functions on the QM/MM boundary atoms (or in the case of plane-waves, just the box size, since all basis functions are nonzero inside the box size) and by monitoring the MM charge in this domain. As we shall illustrate in the next section, the use of chemically accurate basis sets including diffuse functions does not affect the stability of the ADMP dynamics, even when negatively charged molecules are considered as the QM model. This is not the case for plane-wave based implementations, where resorting to more complicated approaches, such as the smearing-out of the MM charges close to the QM region through the use of pseudopotentials, becomes mandatory at any level of accuracy of the basis set.[22] Of course, for abnormally large charges (charges with electron affinity greater than the ionization potential of the QM system), smearing-out of these charges can be a necessity, irrespective of the kind of basis set used, especially when these charges overlap with the physical extent of the basis set.

III. Examples and Discussion

In this section we discuss some test calculations to highlight the capabilities of the ADMP/ONIOM method described above. The purpose of the first few cases is to gauge the stability of the method. We perform some quality checks with respect to the most debated issue in hybrid approaches, namely, the behavior at the QM/MM interface. Hybrid methods can show an intrinsic imbalance between two very different molecular pictures: atomic charges and vdW parameters optimized ad hoc for a self-consistent force field can give poor performances when combined with QM calculations, in particular in evaluating the interactions involved at the QM/MM boundaries. A number of QM/MM approaches produce a poor description for the first solvation shell of a QM molecule or ion embedded in a MM

environment. These problems can be overcome to some degree by an intellingent choice of the model, so that all the important features affecting the phenomenon under study are included and, when possible, to avoid important interactions such as hydrogen bonds and, more general, strong changes in electric polarization at the QM/MM boundaries. These latter requirements cannot be easily fulfilled when charged or strongly polarized QM systems are involved, for example, in biological systems. Furthermore, the inclusion of the MM atomic charges in the QM Hamiltonian can lead also to unphysical effects as discussed earlier, and part of the electronic density can artificially localize on positively charged MM atoms (electronic spill-out). In the case of extended Lagrangian approaches, this can lead to the heating of electrons and can cause unphysical dynamics.[22]

To gauge the ADMP/ONIOM method in these respects, we have simulated the S_N2 reaction of methyl chloride with a chloride ion starting from the $(Cl-CH_3-Cl)^-$ transition state (the model) embedded in a MM water cluster. Due to the excess negative charge, large basis sets are mandatory to allow flexibility in both the radial and the angular part of the electronic distribution, through the inclusion of diffuse and polarization functions, respectively. Therefore such a system is particularly suitable to probe the stability of the method with respect to possible spill-out effects at the interface and over-polarization of the QM wave functions due to the MM charges. It must, however, be noted that the choice of model here (only $(Cl-CH_3-Cl)^-$) is being used to test the ADMP/ONIOM approach and in a full production calculation some of the water molecules surrounding $(Cl-CH_3-Cl)^-$ should probably be included in the model region for the best results.

As a further test we considered the simulation of (i) a chloride ion and (ii) a water molecule, inside an MM water cluster. The latter system may be seen as a prototypical of a hydrogen bonding system treated at the QM/MM level. In both cases the radial distribution functions involving QM and MM atoms was analyzed to gauge the behavior of the ADMP/ONIOM potential at the QM/MM interface.

As a last example in the present study the proton hopping between two water molecules was simulated inside the gramicidin A ion-channel. This example is designed to show the capabilities of the ADMP/ONIOM method in elucidating proton-transfer mechanisms, an essential event in biological chemistry. Proton hopping in transmembrane channels constitutes a challenge for the theoretical description of large systems due to the involvement of extensive hydrogen bond networks and the presence of transmembrane electric fields.

All the ADMP/ONIOM calculations have been performed using a development version of the Gaussian[35] suite of programs, while MD simulations using the DL-Poly[51] program furnished the starting configuration for all systems. The level of theory employed to build the ONIOM potential was density functional theory along with the standard 6-31G(d), 6-31G(d,p), and 6-31+G(d,p) basis sets. In particular, we used the BLYP density functional, combining the Becke[52] exchange terms with the Lee−Yang−Parr[53] correlation functional and the hybrid B3LYP functional, that also includes the Hartree−Fock exchange terms in the same ratios as those optimized by Becke.[54] The AMBER[55] set of parameters together with the TIP3P[56] water model provided for the MM force field.

A. $(Cl-CH_3-Cl)^- \rightarrow Cl^- + CH_3Cl$ in Water Cluster. The nucleophilic substitution (S_N2) reaction ($X^- + CH_3Y \rightarrow Y^- + CH_3X$) is considered as a benchmark reaction in the study of chemical reactivity in aqueous solution.[57,58] However, the purpose of the current study is the demonstration of the ADMP/ONIOM procedure and not the mechanism of the process involved. The isolated transition state $(Cl-CH_3-Cl)^-$ was obtained by a B3LYP/6-31+G(d,p) calculation. This structure was then fixed at the center of a cubic periodic box of length 45 Å with water molecules surrounding the ion, and a classic MD simulation was performed at normal density using the AMBER force field and TIP3P water model. Standard AMBER parameters were used to treat the chloride ion and methyl group. After 100 ps of equilibration, a cluster containing the $(Cl-CH_3-Cl)^-$ subsystem (the model) and the closest 256 water molecules was selected from the simulation box and used as the starting structure in the ADMP/ONIOM simulation.

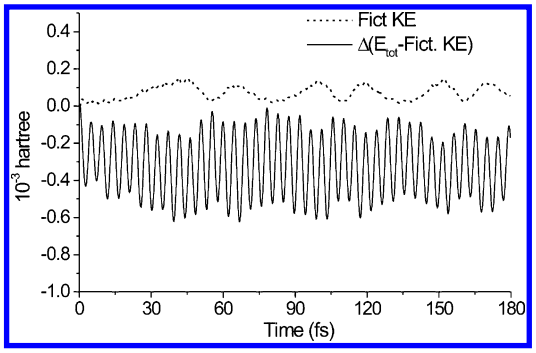

Figure 1. The ADMP/ONIOM trajectory for the $Cl-CH_3-Cl \rightarrow CH_3-Cl + Cl^-$ S_N2 reaction. Time evolution of the fictitious kinetic energy and the change in the difference between the total and the fictitious kinetic energy (10^{-3} au).

To perform the ADMP/ONIOM simulation, the same MM force field was retained while B3LYP/6-31+G(d,p) was the QM level of theory. The core and valence orbitals [for the $(Cl-CH_3-Cl)^-$ subsystem] were weighted differently during the dynamics with $\mu_{valence} = 0.1$ amu bohr$^2 \approx 180$ au for the valence electrons, using the tensorial fictitious mass scheme described in ref 17 to obtain improved adiabatic control. (The tensorial fictitious mass scheme fixes the effective mass of the core electrons based on $\mu_{valence}$ and Fock matrix elements.) The system was simulated in a constant NVE ensemble, and $\Delta t = 0.25$ fs was the time step for a trajectory of 180 fs duration, the time required to get well-separated products.

In Figures 1 and 2, some important parameters reflecting the accuracy of the ADMP trajectory are reported. The fluctuation in the total energy conservation is 0.6 millihartree, which is similar to that found in other full ab-initio ADMP simulations performed using similar values of time step and fictitious mass.[16−18] Furthermore, no significant heating of the density matrix was observed, which indicates that no fraction of the electron density moves artificially to localize on MM atoms. In Figure 2, the Frobenius norm of the Fock and density matrixes commutator, $||[\mathbf{F},\mathbf{P}]||_F$, and the adiabaticity index, $d\mathscr{H}_{fict}/dt$, give a measure of the deviation of the extended Lagrangian trajectory from a Born−Oppenheimer dynamics trajectory.[19] The small order of magnitude of these values demonstrates that the QM/MM combination in the Hamiltonian does not alter the accuracy of the extended Lagrangian dynamics and the dynamics remains close to the corresponding Born−Oppenheimer surface. Hence, in this example, the ADMP/ONIOM approach allows for stable simulations, even in the presence of external fields (treated with an inclusion of point charges in the Hamiltonian) and charged QM systems described by large basis sets.

B. QM Chloride Ion and Water Molecule in an MM Water Cluster. The B3LYP/6-31+G(d,p) level of theory and the AMBER/TIP3P force field was employed to perform an ADMP/ONIOM simulation of a chloride ion embedded in a cluster of 256 water molecules. A procedure analogous to that

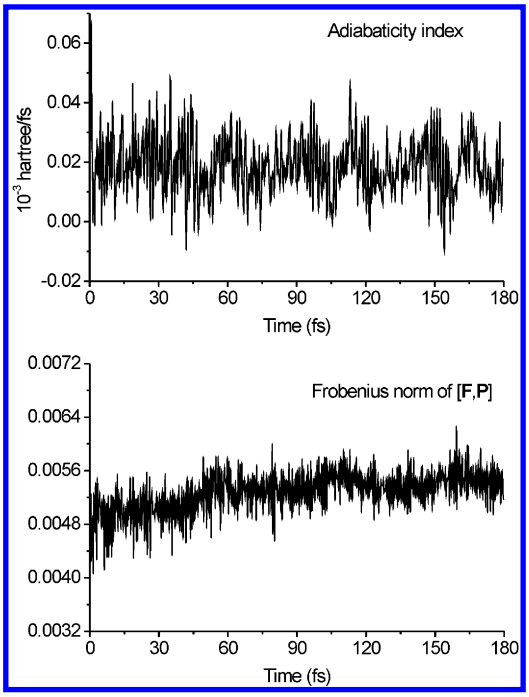

Figure 2. Time evolution of adiabaticity index (in 10^{-3} Hartree/fs) and the Frobenius norm $||[\mathbf{F},\mathbf{P}]||_F$ for the $Cl-CH_3-Cl \rightarrow CH_3Cl + Cl^-$ S_N2 reaction in the ADMP/ONIOM simulation.

adopted for the previous example provided for the starting configuration. The simulation time step was $\Delta t = 0.25$ fs and a valence fictitious mass of $\mu_{\text{valence}} = 0.1$ amu bohr$^2 \approx 180$ au within the tensorial fictitious mass scheme was chosen. Energy and structure data were sampled for 3 ps after ADMP/ONIOM equilibration of 2 ps.

In Figure 3 the chloride−oxygen and the chloride−hydrogen radial distribution functions (RDF) are shown for the ADMP/ONIOM simulation. All RDFs in this paper were calculated in the following fashion. The number of events inside a certain bin-size was calculated from the ADMP trajectory. This number was then divided by the total number of configurations used (indicative of the length of the trajectory), volume inside the spherical shell created by the chosen bin-size, and the number density of the system. The Cl−O RDF shows a maximum at about 3.3 Å, while the first two peaks of the Cl−H RDF are located at about 2.3 and 3.7 Å, respectively. Thus the first solvation shell of the chloride ion is reproduced reasonably well with respect to the experimental values[59] from neutron defraction study of chloride ion in liquid water (3.25 Å for Cl−O, and 2.29 and 3.66 Å for two Cl−H peaks, respectively). Also in this case we observe a good behavior of the parameters governing the dynamics. The total energy is conserved to within 2×10^{-4} hartree, while the maximum value of the fictitious kinetic energy is 1.4×10^{-7} hartree. Furthermore, the adiabaticity index was less than or equal to 2.4×10^{-7} and the Frobenius norm of the Fock and density matrix commutator, [**F**,**P**], had a maximum value of 4.05×10^{-4}, which were both well inside the expected range for retaining adiabatic dynamics. With these results we were able to ascertain that our QM/MM dynamics scheme was stable and the adiabaticity was well-maintained through the dynamics of this test system.

Radial distribution functions involving a model water molecule in a MM water cluster have been studied by other authors at several levels of QM/MM dynamics.[21,60] These RDF generally show shifts with respect to experimental values indicating too strong a QM/MM interaction; in particular an over polarization of the electronic cloud has been indicated as being possibly

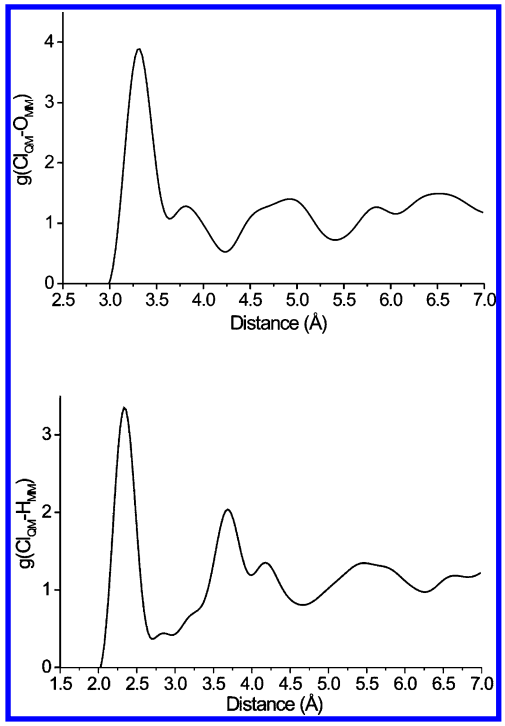

Figure 3. Pair correlation functions for a QM chloride ion (the *model*) embedded in a cluster of 256 MM water molecules. All radial distribution functions in this paper were calculated in the following fashion. The number of events inside a certain bin-size was calculated from the ADMP trajectory. This number was then divided by the total number of configurations used (indicative of the length of the trajectory), volume inside the spherical shell created by the chosen bin-size, and the number density of the system.

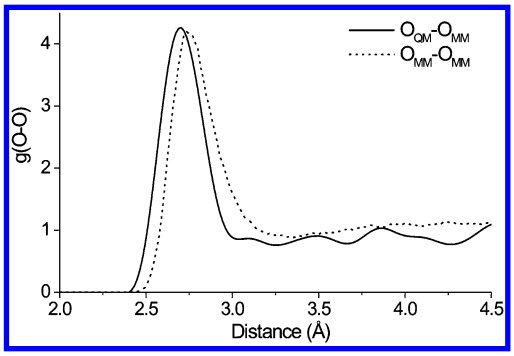

Figure 4. ADMP/ONIOM simulation of a water molecule in a water cluster performed at B3LYP/6-31G(d,p)/Amber level: pair correlation function involving the model oxygen and the oxygens in the surrounding MM molecules (solid line), and pair correlation function of oxygen atoms contained in the MM region (dotted line).

responsible for this trend. An ADMP/ONIOM simulation of a water cluster of 256 molecules was performed in the present work in which the central water of the initial configuration is the model and was treated at the B3LYP/6-31G(d,p) level. The TIP3P potential was employed for the MM level. A classical MD simulation performed for 100 ps at 300 K provided for the starting configuration. Data were then collected for 3 ps at the same temperature after a ADMP/ONIOM equilibration of 2 ps. The simulation time step was $\Delta t = 0.2$ fs and $\mu_{\text{valence}} = 0.1$ amu bohr^2 was employed.

In Figure 4, the RDF between the oxygen of the model and the oxygens belonging to the MM water molecules is compared with the radial distribution function for the oxygen atoms belonging to the water molecules in the MM region. The first peak of the RDF is in very good agreement between the two panels of the figure. Since the TIP3P water model is known to

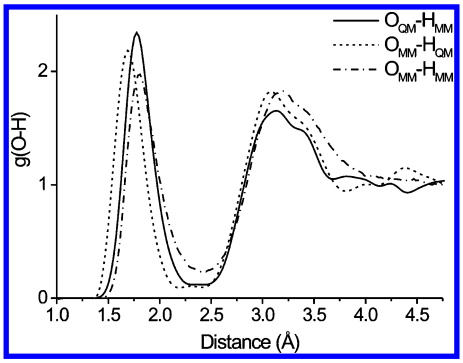

Figure 5. ADMP/ONIOM simulation of a water molecule in a water cluster performed at B3LYP/6-31G(d,p)/Amber level. Pair correlation function involving the model oxygen and the embedding hydrogens (solid) and the model hydrogens and the embedding oxygens (dot−dash) are compared with the pair correlation function for the MM level oxygen and hydrogens (shown using dotted lines).

reproduce the water radial distribution function reasonably accurately, we are inclined to interpret this agreement between the $O_{QM}-O_{MM}$ and $O_{MM}-O_{MM}$ RDFs as indicating that our QM/MM interface does not introduce significant artifacts into our calculations.

In Figure 5 the three possible oxygen−hydrogen RDFs involving the model and the surrounding waters are reported. In this case the picture of the first solvation shell of the QM solute is satisfactory. In Figures 4 and 5, first solvation shell values about 2.7, 1.8, and 1.7 Å for the $O_{QM}-O_{MM}$, $O_{QM}-H_{MM}$, and $H_{QM}-O_{MM}$ distributions are obtained, respectively. Note that these results involving QM and MM atoms are close to those provided by the TIP3P water model (2.72 Å for the oxygen−oxygen and 1.78 Å for the oxygen−hydrogen distances). Thus, there is no apparent evidence of a dramatic overpolarization effect in these cases.

When we compare a hybrid calculation with its full quantum mechanical counterpart, MM charges account for the polarization of the model electronic cloud, while the repulsion between QM and MM atoms is represented by the vdW MM energy terms, and the possible charge transfer between orbitals belonging to MM and QM atoms is naturally absent. The difference with respect to a full ab-initio description relies on this approximation and the performance of hybrid potentials strongly depend on the specific combination of the QM level of theory and MM functionals. Nevertheless, the examples given above demonstrate that the use of standard nonpolarizable force fields within an electronic embedding scheme as depicted in section II can provide well-behaved ADMP/ONIOM dynamics and a reasonable description of the interactions at the QM/MM interface.

C. Proton Transfer in Gramicidin A. As a further test, the mechanism of proton hopping in the transmembrane channel gramicidin A was examined. This system has been considered an important case to elucidate the mechanism of ion transport and has been widely investigated both theoretically and experi-

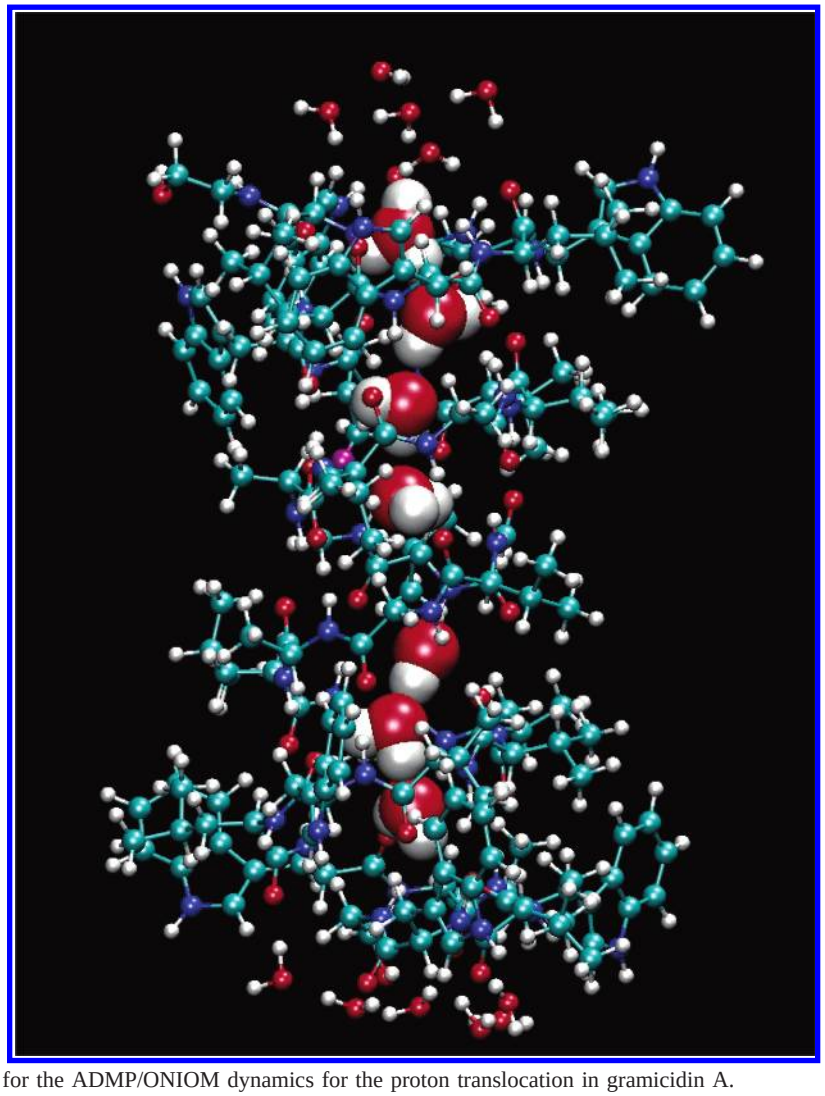

Figure 6. The real system for the ADMP/ONIOM dynamics for the proton translocation in gramicidin A.

mentally. (For a general overview of the computational studies on gramicidin A channel, see ref 61; see also ref 62 for an ab-initio study on a model analogue of gramicidin A.)

The gramicidin A channel is formed by two β helices, each constituted by 15 alternating *D*- and *L*-amino acids. This conformation allows the polar groups of the peptides chain to point inward to the channel, while the hydrophobic side chains are embedded in the transmembrane lipids. Ion transport, in particular the proton Grotthuss mechanism along a water chain accommodated in the channel, involves a highly correlated hydrogen bond network in a strongly polarized system. Furthermore, the application of external electric fields is required to simulate the applied gradient potential during the experiments.

The real system considered here includes the gramicidin A and 18 water molecules for a total of 607 atoms (see Figure 6a). Eight of these water molecules are contained inside the channel, while the remaining water molecules form suitable caps to the channel. The starting configuration for the ADMP/ONIOM dynamics was selected from an equilibrated classical MD simulation using the Multi-State Empirical Valence Bond model.[63−67] This initial structure places the excess proton on the water molecule just inside the channel mouths (water no. 1). The proton translocation is expected to be modulated by the hydrogen bond network involving both the water molecules and the polar groups of the peptidic chain. Hence, the model was chosen to include part of the Gramicidin backbone and the whole set of water molecules. The dangling valences are saturated by link hydrogens atoms. The model includes a total of 156 atoms (see Figure 7. (For the time-scales involved in this study, the proton remained inside the top monomer of the Gramicidin backbone. This justified including only the protein backbone from the top monomer in the model while the bottom monomer was treated within the MM framework.)

Two ADMP/ONIOM simulations were performed using the BLYP/6-31G(d) and the B3LYP/6-31G(d) QM levels together with the AMBER MM force field. Values of $\mu_{\text{valence}} = 0.1$ amu bohr $\approx$ 180 au and $\Delta t = 0.2$ fs were used and a constant temperature of 300 K was enforced by velocity re-scaling every 2 fs. A homogeneous electric field of $2. \times 10^{-4}$ au ($\approx$280 mV) was applied along the channel axis to simulate the gradient of electrostatic potential during the experiments (usually about 200 mV − 400 mV) to drive the proton translocation. Harmonic constraints were employed to fix the position of the oxygens belonging to the capping water molecules.

To proceed further with our discussion we recognize that for the energy expression in eq 1, the interaction of the MM charges with the charges on the model atoms, at the MM level of theory (electronic embedding), occurs in the first two terms of eq 1. However, due to the opposite sign of these terms, these contributions cancel out for almost all atoms in the system. Hence, it is arbitrary what charges are picked for the atoms in the model system during the MM calculation. On account of this, all the atoms in the portion of the model system most susceptible to bond breaking and formation, i.e., the water wire inside the gramicidin channel, were chosen to have zero molecular mechanics charges at both the real MM and model MM calculations. This cancellation works out for all the model atoms except for the ones whose charges are scaled (or set to zero) to avoid over-polarization. (See the discussion in the last paragraph of section II.) The interaction between these "scaled" charges and the model atoms do not cancel between the real and model MM calculations (since the charges are scaled only during the calculation of the second and third terms in eq 1), and it is here that the choice of the model charges could affect the physics of the problem. However, to nullify this effect, care was taken to choose the scaled atoms as the ones that already had small values for charges in the real MM calculation, thus reducing this effect substantially. Furthermore, the effect of scaling does not alter the total charge of the system in a serious fashion, for the same reason discussed above.

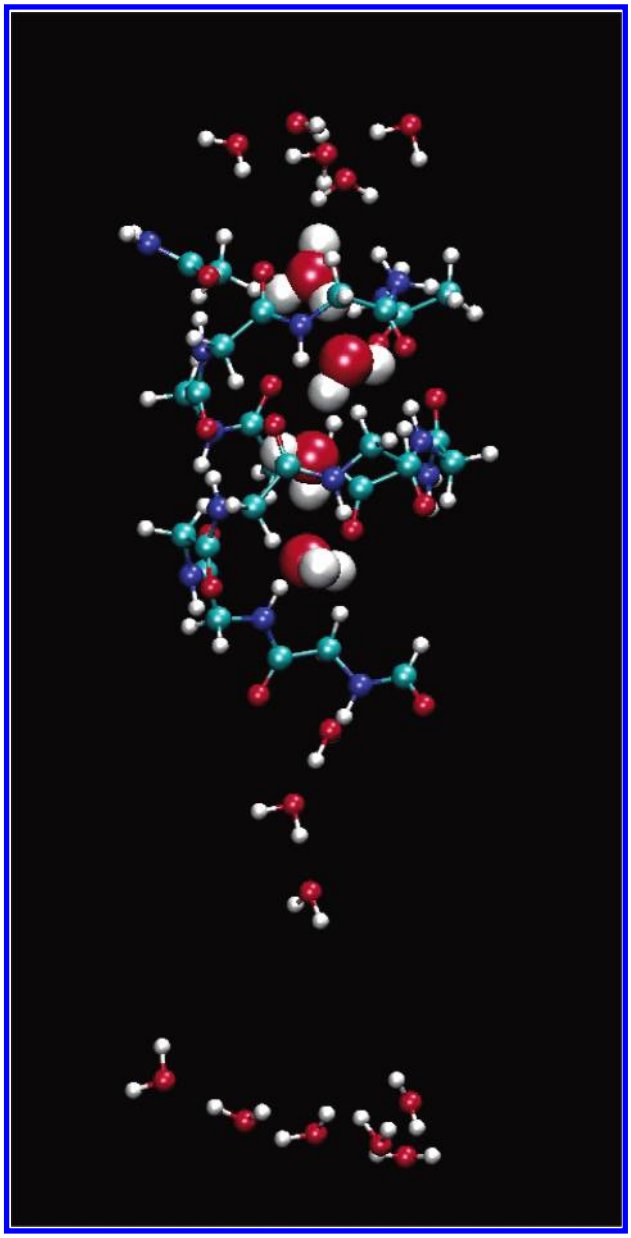

Figure 7. The 156 atom model (QM) system for the ADMP/ONIOM dynamics for the proton translocation in gramicidin A.

The time scales accessible to ab-initio dynamics (on the order of picoseconds) prohibit the simulation of the entire transmembrane protein translocation (on the order of nanoseconds), but it is sufficient to give insights on the intrisic mechanism of the proton hopping. In both simulations, the starting structure has no barrier for the first proton hop and this occurs to water no. 2 inside the gramicidin channel. The excess proton remains localized between water no. 2 and water no. 3 for about half a picosecond. The simulations were stopped when the hop from water no. 2 to water no. 3 was almost complete (500 fs for the BLYP and 650 fs for the B3LYP dynamics, respectively).

In Figures 8−12, the BLYP and B3LYP dynamics are compared. Figure 8 shows the radial distribution of oxygen−oxygen distances of the first four waters inside the channel.

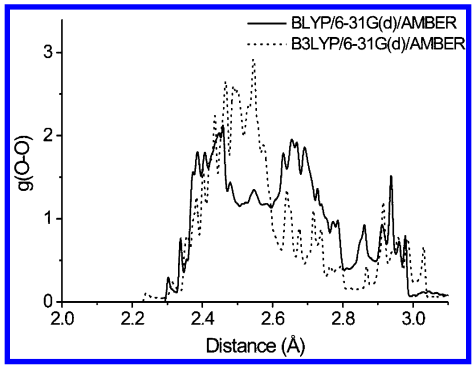

Figure 8. Pair correlation functions for the oxygen−oxygen distances of the first four chain waters inside the Gramicidin channel.

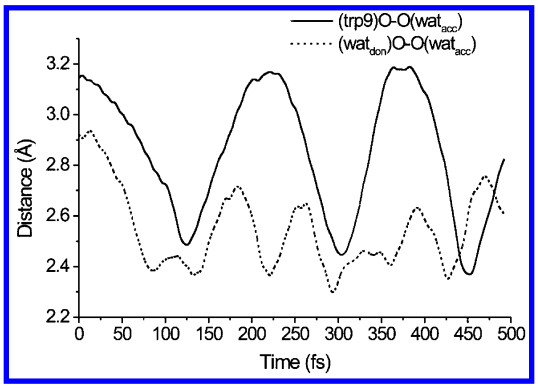

Figure 9. The ADMP/ONIOM trajectory obtained at the BLYP/6-31G(d)/Amber level for the proton translocation in gramicidin A. Progress of the distances between the excess proton and the oxygens of the donor and the acceptor waters, respectively.

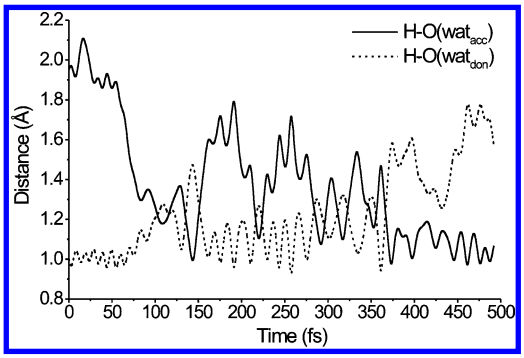

Figure 10. The ADMP/ONIOM trajectory obtained at BLYP/6-31G-(d)/Amber level for the proton translocation in gramicidin A. Progress of the oxygen−oxygen distances between the donor and the acceptor waters and between the acceptor and the carbonyl of tryptophan 9.

Distance values are spread in the range between 2.3 and 3.0 Å with a large distribution between 2.45 and 2.7 Å. These values are similar to those seen for the Zundel-like ($H_5O_2^+$) and the Eigen-like ($H_9O_4^+$) protonated complex present in bulk water. The Eigen-like arrangement can be obtained in this case with the channel carbonyl groups completing the necessary hydrogen bond network. It is worth noting that the distribution obtained with the BLYP functional shows a larger contribution corresponding to the Eigen complex as compared to that found using B3LYP, where in the latter case the distribution is mostly concentrated on values below 2.6 Å. This difference between levels of DFT treatment is in agreement with that observed in previous ADMP studies of protonated water clusters.[68]

In Figures 9−12, we compare the BLYP and the B3LYP behavior in the time evolution of some atomic distances of interest. In Figures 9 and 11 we show the distances between

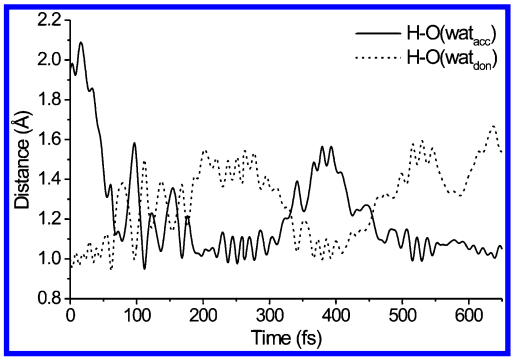

Figure 11. The ADMP/ONIOM trajectory obtained at B3LYP/6-31G-(d)/Amber level for the proton translocation in gramicidin A. Progress of the distances between the excess proton and the oxygens of the donor and the acceptor waters, respectively.

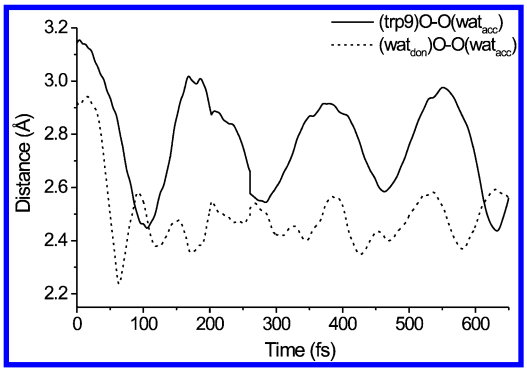

Figure 12. The ADMP/ONIOM trajectory obtained at B3LYP/6-31G-(d)/Amber level for the proton translocation in gramicidin A. Progress of the oxygen−oxygen distances between the donor and the acceptor waters and between the acceptor and the carbonyl of tryptophan 9.

the excess proton and the oxygens belonging to the second and the third water (the donor and the acceptor, respectively, for the majority of the trajectory). Figures 10 and 12 show the oxygen−oxygen distances between the donor and the acceptor waters together with the distance between the acceptor oxygen and its solvating carbonyl, namely, from the tryptophan 9 along the gramicidin peptide chain.

Note that in the BLYP case the transient proton approaches the acceptor water around 100 fs, but most of the time it is located on the donor water. Temporary hops to the acceptor occur when the donor water is close to the acceptor (wat$_{don}$)O−O(wat$_{acc}$), compare Figures 9 and 10. Also, when the Trp9-(C)O−O(wat$_{acc}$) distance is less than 2.65 Å, there is a noticeable decrease of the (wat$_{don}$)O−O(wat$_{acc}$) motion amplitude, leading to an oxygen−oxygen distance closer to a Zundel-like value (≈2.4 Å). During one of these events, the final hopping to the acceptor water molecule occurs (at about 350 fs). Interestingly, after about 300 fs, the motion of the excess proton seems less correlated with the motion of the carbonyl group hydrogen binding to the acceptor oxygen. This suggests that other factors may come into play toward the end of the proton hop to stabilize the event.

A different trend is observed when the results from the dynamics performed at the B3LYP level are considered. Here the oxygen−oxygen distance of the donor and the acceptor waters evolves according to a Zundel-like arrangement along the whole trajectory, and the excess proton is localized on both the donor and the acceptor over time (see Figures 11 and 12). Furthermore, the Trp9(C)O−O(wat$_{acc}$) distance show values below 2.9 Å for most of the time, and the correlation of motions involving the protonated complex and the solvating tryptophan carbonyl is less evident.

The short time scale investigated here and the small statistical sample prohibit general conclusions on the comparison of the two DFT functionals considered, although there do appear to be qualitative differences between the two levels of DFT in describing the proton hopping dynamics. A more comprehensive study of the proton hopping dynamics and the differences between levels of DFT will be the topic of future research.

IV. Concluding Remarks

In this paper, a new methodology has been presented to perform hybrid ab-initio/empirical molecular dynamics. The method combines the hybrid ONIOM scheme with the ADMP methodology, in which the one-electron density matrix, as expanded in an atom-centered Gaussian basis set, is propagated using fictitious variables within an extended Lagrangian approach.

The resulting ADMP/ONIOM formalism has been analyzed for the general case, including the presence of link atoms to saturate dangling valences and a standard electronic embedding scheme to describe the electrostatic interactions between the QM and the MM parts. In this work, a nonpolarizable MM force field was assumed, but generalization to polarizable MM forcefields is clearly possible. Since the link atom positions are fully defined by the coordinates of the real system, a unique definition of the ONIOM potential exists that is single-valued and differentiable with respect to the real coordinates **R**, thus allowing conservative dynamics to be performed. Due to the integrated expressions of the ONIOM energy and energy derivatives, a formal identity with the Lagrangian is obtained governing the ab-initio dynamics. This identity also holds for the analysis of the deviations from the Born−Oppenheimer surface. The combination of hybrid terms within the forces was analyzed in detail. The force acting on the density matrix is seen to have the same analytical form as in full ab-initio ADMP. However, it is affected by the MM environment via the Fock matrix **F**, including the electrostatic interactions with the MM region.

To test the ADMP/ONIOM method for possible unphysical interactions between the QM electronic density and the MM nuclei in proximity to the QM/MM boundary, the S_N2 reaction of methyl chloride plus a chloride ion was simulated starting from the $(Cl-CH_3-Cl)^-$ transition state (the model) embedded in a MM water cluster. Due to the excess negative charge, the standard 6-31+G(d,p) basis set was adopted, including diffuse and polarization functions. The total energy was well conserved during the dynamics, and the fictitious kinetic energy remained very small, indicating that no significant heating of the density matrix occurs. Furthermore, adiabatic control indices demonstrated that the QM/MM combination in the Hamiltonian does not alter the adiabaticity of the extended Lagrangian dynamics. Hence, the localized picture provided by the electronic expansion over an atom-centered basis set appears to allow for well-behaved simulations even when chemically accurate basis sets for charged systems are employed, together with a standard electronic embedding scheme to describe QM/MM interactions. The simulation in a MM water cluster of a QM chloride ion and a QM water molecule were also carried out. RDFs obtained for the distances involving QM and MM atoms also indicate a reasonable description of the interactions at the QM/MM interface.

As a more complicated preliminary application, the results from BLYP and the hybrid B3LYP functionals were compared in two analogous simulations of a proton hopping between two water molecules inside the gramicidin A channel. In the BLYP case, a transfer mechanism was observed via the formation of an Eigen-like complex involving a carbonyl group solvating the acceptor water. In the B3LYP case, the formation of the Eigen-like complex is less probable and the correlation of motions involving the protonated complex and the peptidic carbonyl less evident. The implementation and testing of the hybrid ADMP/ONIOM methodology for a variety of complex systems will be the topic of future research.

Acknowledgment. This work was supported by the Office of Naval Research (G.A.V.), the National Science Foundation Grant CHE-0131157 (H.B.S.), and Gaussian, Inc. An allocation of computer time from the Center of High Performance Computing at the University of Utah is gratefully acknowledged. We also thank Ms. Stephanie Atherton for her help in using the MS-EVB-DL-POLY code.

References and Notes

(1) Warshel, A.; Levitt, M. *J. Mol. Biol.* **1976**, *103*, 227.
(2) Singh, B.; Kollman, P. A. *J. Comput. Chem.* **1986**, *7*, 718.
(3) Field, C.; Bash, P. A.; Karplus, M. *J. Comput. Chem.* **1990**, *11*, 700.
(4) Stanton, R. V.; Hartsough, D. S.; Merz, K. M. *J. Comput. Chem.* **1994**, *16*, 113.
(5) Stanton, R. V.; Little, L. R.; Merz, K. M. *J. Phys. Chem.* **1995**, 17344.
(6) Alhambra, C.; Byun, K.; Gao, J. In *Combined Quantum Mechanical and Molecular Mechanics Methods*; Gao, J., Thompson, M., Eds.; number 712 in ACS Symposium Series, 1999; page 35.
(7) Gao, J. *Acc. Chem. Res.* **1996**, *29*, 298.
(8) Alhambra, C.; Wu, L.; Zhang, Z.; Gao, J. *J. Am. Chem. Soc.* **1998**, *120*, 3858.
(9) Ferenczy, G. G.; Rivail, J.-L.; Surjan, P. R.; Naray-Szabo, G. *J. Comput. Chem.* **1992**, *13*, 830.
(10) Gao, J.; Amara, P.; Alhambra, C.; Field, M. *J. Phys. Chem. A* **1998**, *102*, 4714.
(11) Andersen, H. C. *J. Chem. Phys.* **1980**, *72*, 2384−2393.
(12) Parrinello, M.; Rahman, A. *Phys. Rev. Lett.* **1980**, *45*, 1196−1199.
(13) Car, R.; Parrinello, M. *Phys. Rev. Lett.* **1985**, *55*, 2471.
(14) Remler, D. K.; Madden, P. A. *Mol. Phys.* **1990**, *70*, 921.
(15) Marx, D.; Hutter, J. John vonNeumann Institute for Computing: Julich, 2000; Vol. 1, Chapter: Ab Initio Molecular Dynamics: Theory and Implementation, p 301.
(16) Schlegel, H. B.; Millam, J. M.; Iyengar, S. S.; Voth, G. A.; Daniels, A. D.; Scuseria, G. E.; Frisch, M. J. *J. Chem. Phys.* **2001**, *114*, 9758.
(17) Iyengar, S. S.; Schlegel, H. B.; Millam, J. M.; Voth, G. A.; Scuseria, G. E.; Frisch, M. J. *J. Chem. Phys.* **2001**, *115*, 10291.
(18) Schlegel, H. B.; Iyengar, S. S.; Li, X.; Millam, J. M.; Voth, G. A.; Scuseria, G. E.; Frisch, M. J. *J. Chem. Phys.* **2002**, *117*, 8694.
(19) Iyengar, S. S.; Schlegel, H. B.; Voth, G. A.; Millam, J. M.; Scuseria, G. E.; Frisch, M. J. *Isr. J. Chem.* **2002**, *42*, 191−202.
(20) Iyengar, S. S.; Schlegel, H. B.; Voth, G. A. *J. Phys. Chem. A* **2003**, *107*, 7269−7277.
(21) Eichinger, M.; Tavan, P.; Hutter, J.; Parrinello, M. *J. Chem. Phys.* **1999**, *110*, 10452.
(22) Laio, A.; VandeVondele, J.; Röthlisberger, U. *J. Chem. Phys.* **2002**, *116*, 6941−6947.
(23) Woo, T. K.; P, M. M.; Deng, L.; Ziegler, T. In *Combined Quantum Mechanical and Molecular Mechanics Methods*; Gao, J., Thompson, M., Eds.; number 712 in ACS Symposium Series, 1999; page 128.
(24) Woo, T. K.; Cavallo, L.; Ziegler, T. *Theor. Chem. Acc.* **1998**, *100*, 307.
(25) Maseras, F.; Morokuma, K. *J. Comput. Chem.* **1995**, *16*, 1170−1179.
(26) Humbel, S.; Sieber, S.; Morokuma, K. *J. Chem. Phys.* **1996**, *105*, 1959.
(27) Svensson, M.; Humbel, S.; Froese, R. D. J.; Matsubara, T.; Sieber, S.; Morokuma, K. *J. Phys. Chem.* **1996**, *100*, 19357.
(28) Svensson, M.; Humbel, S.; Morokuma, K. *J. Chem. Phys.* **1996**, *105*, 3654.
(29) Dapprich, S.; Komaromi, I.; Byun, K. S.; Morokuma, K.; Frisch, M. J. *J. Theochem. J. Mol. Struct.* **1999**, *462*, 1.
(30) Maseras, F. *Top. Organomet. Chem.* **1999**, *4*, 165.
(31) Vreven, T.; Morokuma, K. *J. Comput. Chem.* **2000**, *21*, 1419−1432.
(32) Vreven, T.; Morokuma, K.; Farkas, O.; Schlegel, H. B.; Frisch, M. J. *J. Comput. Chem.* **2003**, *24*, 760.
(33) Vreven, T.; Morokuma, K. *Theor. Chem. Acc.* **2003**, *109*, 125.

(34) Kerdcharoen, T.; Morokuma, K. *Chem. Phys. Lett.* **2002**, *355*, 257.
(35) Frisch, M. J.; Trucks, G. W.; Schlegel, H. B.; Scuseria, G. E.; Robb, M. A.; Cheeseman, J. R.; Montgomery, J. A., Jr.; Vreven, T.; Kudin, K. N.; Burant, J. C.; Millam, J. M.; Iyengar, S. S.; Tomasi, J.; Barone, V.; Mennucci, B.; Cossi, M.; Scalmani, G.; Rega, N.; Petersson, G. A.; Nakatsuji, H.; Hada, M.; Ehara, M.; Toyota, K.; Fukuda, R.; Hasegawa, J.; Ishida, M.; Nakajima, T.; Honda, Y.; Kitao, O.; Nakai, H.; Klene, M.; Li, X.; Knox, J. E.; Hratchian, H. P.; Cross, J. B.; Adamo, C.; Jaramillo, J.; Gomperts, R.; Stratmann, R. E.; Yazyev, O.; Austin, A. J.; Cammi, R.; Pomelli, C.; Ochterski, J. W.; Ayala, P. Y.; Morokuma, K.; Voth, G. A.; Salvador, P.; Dannenberg, J. J.; Zakrzewski, V. G.; Dapprich, S.; Daniels, A. D.; Strain, M. C.; Farkas, O.; Malick, D. K.; Rabuck, A. D.; Raghavachari, K.; Foresman, J. B.; Ortiz, J. V.; Cui, Q.; Baboul, A. G.; Clifford, S.; Cioslowski, J.; Stefanov, B. B.; Liu, G.; Liashenko, A.; Piskorz, P.; Komaromi, I.; Martin, R. L.; Fox, D. J.; Keith, T.; Al-Laham, M. A.; Peng, C. Y.; Nanayakkara, A.; Challacombe, M.; Gill, P. M. W.; Johnson, B.; Chen, W.; Wong, M. W.; Gonzalez, C.; Pople, J. A. *Gaussian 03*, Rev. B.02; Gaussian, Inc.: Pittsburgh, PA, 2003.
(36) Scuseria, G. E. *J. Phys. Chem. A* **1999**, *103*, 4782.
(37) Blöchl. *Phys. Rev. B* **1994**, *50*, 17953−17979.
(38) Lippert, G.; Hutter, J.; Parrinello, M. *Theor. Chem. Acc.* **1999**, *103*, 124.
(39) Lippert, G.; Hutter, J.; Parrinello, M. *Mol. Phys.* **1997**, *92*, 477.
(40) Sharma, M.; Wu, Y.; Car, R. *Int. J. Quantum Chem.* **2003**, *95*, 821−829.
(41) Kohn, W. *Phys. Rev.* **1959**, *115*, 809−821.
(42) Marzari, N.; Vanderbilt, D. *Phys. Rev. B* **1997**, *56*, 12847−12865.
(43) Martyna, G.; Cheng, C.; Klein, M. L. *J. Chem. Phys.* **1991**, *95*, 1318.
(44) Murphy, R. B.; Philipp, D. M.; Friesner, R. A. *J. Comput. Chem.* **2000**, *21*, 1442.
(45) Gordon, M. S.; Freitag, M. A.; Bandyopadhyay, P.; Jensen, J. H.; Kairys, V.; Stevens, W. J. *J. Phys. Chem. A* **2001**, *105*, 293−307.
(46) Bakowies, D.; Thiel, W. *J. Phys. Chem.* **1996**, *100*, 10580.
(47) Golub, G. H.; van Loan, C. F. *Matrix Computations*; The Johns Hopkins University Press: Baltimore, 1996.
(48) Swope, W. C.; Andersen, H. C.; Berens, P. H.; Wilson, K. R. *J. Chem. Phys.* **1982**, *76*, 637.
(49) Reuter, N.; Dejaegere, A.; Maigret, B.; Karplus, M. *J. Phys. Chem. A* **2000**, *104*, 1720.
(50) Sherwood, E. John vonNeumann Institute for Computing, Julich, 2000; Vol. 1; Chapter: Hybrid Quantum Mechanics/Molecular Mechanics Approaches.
(51) Smith, W.; Forester, T. R. Dl_poly is a package of molecular simulation routines. Copyright the council for the central laboratory of the research councils, Daresbury Laboratory at Daresbury, nr. Warrington, 1999.
(52) Becke, A. D. *J. Chem. Phys.* **1988**, *38*, 3098.
(53) Lee, C.; Yang, W.; Parr, R. G. *Phys. Rev. B* **1988**, *37*, 785.
(54) Becke, A. D. *J. Chem. Phys.* **1993**, *98*.
(55) Cornell, W. D.; Cieplak, P.; Bayly, C. B.; Gould, I. R.; Mertz, K. M., Jr.; Ferguson, D. M.; Spellmeyer, D. S.; Fox, T.; Caldwell, J. W.; Kollman, P. A. *J. Am. Chem. Soc.* **1995**, *117*, 5179.
(56) Jorgensen, W. L.; Chandrasekhar, J.; Madura, J. D.; Impey, R. W.; Klein, M. L. *J. Chem. Phys.* **1983**, *79*, 926−935.
(57) Hori, T.; Takahaschi, H.; Nitta, T. *J. Comput. Chem.* **2002**, *24*, 209.
(58) Re, S.; Morokuma, K. *J. Phys. Chem. A* **2001**, *105*, 7185.
(59) Yamagami, M.; Wakita, H.; Yamaguchi, T. *J. Chem. Phys.* **1995**, *103*, 8174.
(60) Tu, Y.; Laaksonen, A. *J. Chem. Phys.* **1999**, *111*, 7519.
(61) Roux, B. *Acc. Chem. Res.* **2002**, *202*, 366.
(62) Sagnella, D. E.; Laasonen, K.; Klein, M. L. *Biophys. J.* **1996**, *71*, 1172.
(63) Schmitt, U. W.; Voth, G. A. *J. Chem. Phys.* **1999**, *111*, 9361.
(64) Schmitt, U. W.; Voth, G. A. *J. Phys. Chem. B* **1998**, *102*, 5547.
(65) Schmitt, U. W.; Voth, G. A. *Isr. J. Chem.* **1999**, *39*, 483.
(66) Cuma, M.; Schmitt, U. W.; Voth, G. A. *J. Phys. Chem. A* **2001**, *105*, 2814−2823.
(67) Day, T. J. F.; Schmitt, U. W.; Voth, G. A. *J. Am. Chem. Soc.* **2000**, *122* (48), 12027.
(68) Iyengar, S. S.; Day, T. J. F.; Petersen, M. K.; Burnham, C. J.; Voth, G. A. *Nature*, submitted.